Engineering Failure Analysis 130 (2021) 105764

Contents lists available at ScienceDirect

Engineering Failure Analysis

journal homepage: www.elsevier.com/locate/engfailanal

Nonlinear three-dimensional anisotropic material model for failure analysis of timber

Hooman Eslami, Laddu Bhagya Jayasinghe, Daniele Waldmann *

Faculty of Science, Technology and Medicine (FSTM), University of Luxembourg, L-4364 Esch-sur-Alzette, Luxembourg

A R T I C L E I N F O

Keywords:
Constitutive model
Elastoplastic orthotropic material
Numerical finite element simulation in ABAQUS
Timber

A B S T R A C T

In this paper, a constitutive material model is proposed to model the nonlinear mechanical response of timber, as elastoplastic orthotropic material under three-dimensional (3D) stress state. An associated flow rule model based on Hoffmann yield criterion and plastic potential is adopted for describing the plasticity of timber under compression. Isotropic strain hardening during plastic deformation is incorporated into Hoffman yield criterion by assuming that equivalent yield stress is a function of the equivalent plastic strain. A stress-based continuum damage formulation with four independent failure criteria in tension and compression is used. The proposed model is implemented as a user material subroutine UMAT in ABAQUS. The results obtained in numerical simulations are evaluated and compared with experimental results. A good agreement has been found between numerical simulations and the experimental results. Therefore, the proposed constitutive model can be used further in numerical simulations of the anisotropic behavior of timber.

1. Introduction

In the last years, timber has been increasingly used as a construction material due to high strength to weight ratio while being in parallel reputed to make an essential contribution to a sustainable future by its positive environmental impact. Since timber products have a good load-bearing capacity under both compression and tension, they can be used for a variety of structural components. Timber is a fully renewable resource as well as it has a low carbon footprint and high carbon storage capacity, and at the end of its life cycle it can be reused or recycled more sustainably compared to other construction materials like steel and concrete [1,2]. Due to its major benefits in sustainability, timber has been noticed rapid development as structural and non-structural components in the construction industry in the last decades, not least as a result of the EU shifts towards environmentally sustainable building practices.

Timber is usually a heterogeneous and orthotropic material that exhibits different constitutive relationship of the material in tension and compression. Although natural imperfections such as knots and resin pockets are not generally considered in numerical modelling, predicting the mechanical behavior of timber is still complicated because of its structure. Timber has unique and independent mechanical properties in three mutually perpendicular axes, defined by the grain direction: longitudinal (parallel to the grain), radial, and tangential [3]. Furthermore, the mechanical properties of timber including strength, modulus of elasticity, shear modulus, and Poisson ratio vary not only by direction but also by the sign of the stress, whether in tension or compression [4]. The behavior in compression parallel to the grain direction is rather linear elastic followed by a ductile failure. In compression

* Corresponding author.
E-mail address: daniele.waldmann@uni.lu (D. Waldmann).

https://doi.org/10.1016/j.engfailanal.2021.105764
Received 20 April 2021; Received in revised form 6 September 2021; Accepted 17 September 2021
Available online 23 September 2021
1350-6307/

perpendicular to the grain, timber shows a plastic behavior with moderate hardening. Under tension, timber shows a linear elastic response followed by a brittle failure in both parallel and perpendicular to the grain direction [4]. Also, it is noticeable that the stiffness and strength properties perpendicular to the grain are much lower than the ones parallel to the grain [5,6].

In order to develop a numerical model of timber structures, it is essential to understand its mechanical behavior. During the last decades, many material models have been developed to define a constitutive law for the complicated behavior of timber, but most of them are only applicable for 2D finite element (FE) analysis [7–10]. Some earlier efforts to calculate the load-carrying capacity of dowel-type timber joints were done by some researchers [11–14]. They developed material models to simulate the brittle failure of timber by studying the initiation of fracture and its growth based on Linear Elastic Fracture Mechanics (LEFM) and Non-linear Fracture Mechanics (NLFM). These studies mostly considered a 2D constitutive model of timber which was only applicable for timber parts with small thickness. Chen et al. [8] Developed a plane stress nonlinear material model to predict the failure of dowel type joints with a failure criterion consisting of tensile stress perpendicular to the wood grains and shear stress parallel to the wood grains. In another approach to investigate the mechanical performance of dowel-type timber joints, a 3D FE model was developed by Santos et al. [15]. However, the timber material model was limited to an orthotropic elastic constitutive law.

The timber material models which were developed to simulate the non-linear behavior of timber can be categorized into three groups: Elastic-plastic models, elastic-damage models and elastic–plastic in combination with damage models [16,17].

In the first group, some studies considered bilinear [18,19] and trilinear [20] stress–strain curves to describe the non-linear behavior of timber under compression perpendicular to the grain. Several other studies in the first group considered the classical flow theory of plasticity in combination with single-surface isotropic yield criteria such as Hill's criterion [21], Tsai-Wu criterion [22] and Hoffman criterion [23].

Kharouf et al. [9] proposed a 2D orthotropic material model according to Hill's yield criterion associated with anisotropic hardening to model the behavior of timber under compression. However, the model did not consider the brittle failure under tension and shear stresses. Dias et al. [18] presented a model that makes no distinction between the radial and tangential behavior of timber and used orthotropic yield criterion based on Hill's criterion associated with isotropic hardening to define a linear elastic–plastic behavior for timber with different stress potentials in different directions. However, this model did not realize any difference between the yield strength of timber in compression and tension and assumed linear elastic-perfect plastic behavior for all the stress cases. Oudjene and Khalifa [24] presented an anisotropic elastic–plastic constitutive law with hardening also based on Hill's criterion and without distinction between radial and tangential properties. In this model, the strength difference of timber in compression and tension, the brittle behavior in tension, and densification in compression were applied. Bouchair and Vergne [25] and Clouston and Lam [26] used Tsai-Wu criterion to develop a 2D FE model of timber. Xu et al. [27] use the Hoffman failure criterion associated with the Hill criterion to develop an orthotropic 3D constitutive model for timber based on the elastic-perfect plastic behavior. However, the elastic or elastic-perfect plastic orthotropic material model cannot retrace the load-deformation behavior of timber accurately.

These single-surface yield criteria are not able to effectively predict the different failure modes that occur in materials like timber [28]. To overcome this shortage, researchers [29–32] proposed multi-surface plasticity criteria. In these criteria, different yield surfaces are combined to make the global failure surface considering the mode of failure in timber. Although the multi-surface criteria are more accurate compared to single surface ones in simulating the different failure modes of timber, they have limitations in usage due to complicated constitutive laws and the possibility of numerical instabilities [28,33].

The second group of models [28,33–35] use Continuum Damage Mechanics (CDM) to model the behavior of timber. The CDM method is a simple approach to implement softening and hardening behavior of timber into the model. In comparison to plasticity, damage is much easier to implement in material models. In this method, the material behavior is completely defined by the damage variables which are inserted into fundamental Hooke's equation to reduce the stiffness matrix. Garib et al. [28] used CDM theory to model stiffness degradation in various stress components and to study the nonlinear behavior under a multi-directional stress state. Sandhaas and Van de Kuilen [34] developed a 3D anisotropic CDM model which is based on eight types of stress-based failure criteria governed by six damage variables. However, no damage interactions were modelled in this model.

The third group of models [36–39] combine the plasticity and different damage models. Most of these models use Hill's criterion as yield surface and damage criteria. Xu et al. [36] developed a timber model includes the anisotropic plasticity coupled with isotropic hardening according to Hill yield criterion to describe the compressive behavior of timber. To describe the brittle behavior in tension and shear, the evolution of damage was modelled by using a reduction of elastic modulus and element removal which is based on modified Hill failure criterion. Khelifa et al. [38] developed a new timber model within the framework of plasticity coupled with CDM which incorporates effects of anisotropic plasticity with isotropic hardening, isotropic damage and large plastic deformations. However, the model uses only one Hill's criterion as plasticity and damage criteria, and does not consider different strength parameters for tension and compression. It is also failed to capture the anisotropic damage developed in timber beams. Later, Sirumbal-Zapata et al. [4] developed a model to represent the cyclic behavior of timber using the Hofmann criterion for plasticity and the Hill criterion for damage. However, since an isotropic damage was assumed in order to maintain a symmetric stress tensor, the individual failure modes could not be identified. Benvenuti et al. [16] proposed a multi-surface elastic-damaging-plastic constitutive model whereas two plastic activation functions and three damage variables were defined. This constitutive model was found effective in ductile and brittle failure modes [40]. However, to simplify the development of the proposed model, the model was restricted only to plane stress cases.

When performing FE analysis on timber structures, or the constitutive relationship of timber, previous studies have simplified timber material as anisotropic or orthotropic elastic materials [15,41–43]. They also do not distinguish the behavior under tension and compression. Many of them do not consider material damage [18,19] or simply the damage as isotropic [4,38]. In addition, several studies set the material stiffness when the stress state reaches the strength criterion [27,36]. Based on the characteristics of timber's complex anisotropic materials, this paper attempts to establish a constitutive model that can simulate the complex mechanical properties of wood.

Thus, in this paper, a constitutive relationship is adopted for timber material based on the isotropic hardening elastoplastic model using the Hoffman yield criterion, which is an extension of Hill's criterion. The proposed material model for timber has the characteristics such as: 1) an orthotropic stress–strain relationship is used in the linear phase; 2) an associated flow rule model based on Hoffman yield criterion and plastic potential is used for describing the plasticity under compression; 3) isotropic strain hardening, which is incorporated into the Hoffman yield criterion, is applied using a hardening modulus to incorporate timber plastic flow in the proposed material model under compression; 4) a stress-based continuum damage formulation with four independent failure criteria in tension and compression is used; 5) three different tensile damages in the grain longitudinal, radial and tangential directions are established using the damage factors and fracture energies. Thus, this elastoplastic model is capable of simulating the brittle behavior of timber in tension and ductile yielding of timber under compression.

The proposed material model can be easily implemented as a user material subroutine (UMAT) in ABAQUS [44] commercial FE analysis software. The developed material model is presented in Section 2, and its implementation in ABAQUS is described in Section 3. Subsequently, this material model is validated by comparison of results to some experimental results, and it is presented in Section 4, followed by the conclusion of the study.

2. The constitutive material model

2.1. Orthotropic linear-elastic constitutive behavior

The constitutive relationship reflects the relationship between stress and strain. In the elastic stage, the stress–strain relationship of an orthotropic material can be written as:

$$\sigma = E\varepsilon_e \tag{1}$$

where σ and ε_e are the applied stress and corresponding elastic strain tensors, respectively. E is the orthotropic elastic matrix which is given as:

$$E = \begin{bmatrix} E_{11} & E_{12} & E_{13} & 0 & 0 & 0 \\ E_{21} & E_{22} & E_{23} & 0 & 0 & 0 \\ E_{31} & E_{32} & E_{33} & 0 & 0 & 0 \\ 0 & 0 & 0 & E_{44} & 0 & 0 \\ 0 & 0 & 0 & 0 & E_{55} & 0 \\ 0 & 0 & 0 & 0 & 0 & E_{66} \end{bmatrix} \tag{2}$$

$$\text{where } E_{11} = (E_1/\beta)\ (1 \ - -\upsilon_{23}.\upsilon_{32}); \quad E_{12} = (E_1/\beta)\ (\upsilon_{21} + \upsilon_{23}.\upsilon_{31}); \quad E_{13} = (E_1/\beta)\ (\upsilon_{31} + \upsilon_{21}.\upsilon_{32}) \tag{3}$$

$$E_{21} = (E_2/\beta)\ (\upsilon_{12} + \upsilon_{13}.\upsilon_{32}); \quad E_{22} = (E_2/\beta)\ (1 \ - -\upsilon_{13}.\upsilon_{31}); \quad E_{23} = (E_2/\beta)\ (\upsilon_{32} + \upsilon_{12}.\upsilon_{13}) \tag{4}$$

$$E_{31} = (E_3/\beta)\ (\upsilon_{13} + \upsilon_{12}.\upsilon_{23}); \quad E_{32} = (E_3/\beta)\ (\upsilon_{23} + \upsilon_{21}.\upsilon_{13}); \quad E_{33} = (E_3/\beta)\ (1 \ - -\upsilon_{12}.\upsilon_{21}) \tag{5}$$

$$E_{44} = G_{12}; \quad E_{55} = G_{13}; \quad E_{66} = G_{23} \tag{6}$$

$$\beta = 1 - (\upsilon_{12}.\upsilon_{21}) - (\upsilon_{13}.\upsilon_{31}) - (\upsilon_{23}.\upsilon_{32}) - (\upsilon_{12}.\upsilon_{23}.\upsilon_{31}) - (\upsilon_{13}.\upsilon_{21}.\upsilon_{32}) \tag{7}$$

where E_i represent the Young's moduli in the three orthotropic directions, υ_{ij} and G_{ij} are the Poisson's ratio and shear moduli, respectively. Direction 1 is the direction parallel to the grain (longitudinal) and directions 2 and 3 are the radial and tangential directions.

Since the elastic matrix relating the stresses and strains is symmetric, the constants are $\upsilon_{21} = \upsilon_{21}(E_2/E_1)$, $\upsilon_{31} = \upsilon_{31}(E_3/E_1)$ and $\upsilon_{32} = \upsilon_{23}(E_3/E_2)$.

2.2. Elastoplastic constitutive behavior

The behavior of elastoplastic materials can be analyzed by constitutive equations which relate the stress to the incremental formulation of strain and other internal variables. For most materials, under monotonic loading, there is a certain limit stress value σ_e, when the stress is lower than σ_e, the deformation of material will be elastic. When the stress reaches the limit stress value, the material begins to enter the elastoplastic state. If the load is kept increasing, a permanent plastic deformation is observed after the release of the load. If the material deforms at constant stress after the stress reached the limit value σ_e, the material is called ideally elastoplastic. Conversely, if the stress reaches σ_e, while the stress still generally increases with increasing deformation, it is called strain hardening. For a strain-hardening material, the limit stress σ_e is a function of the plastic strain ε_p, which can be expressed in a general form as:

$$\sigma_{ek} = \sigma_e(\varepsilon_p) \tag{8}$$

According to the theory of plasticity, the total strain ε can be divided into an elastic component ε_e and a plastic component ε_p.

$$\varepsilon = \varepsilon_e + \varepsilon_p \tag{9}$$

Since the plastic deformation is related to the deformation history, it is more convenient to give the constitutive relationship reflecting the plastic stress–strain relationship in the form of strain increment. The theory of expressing plastic constitutive relationship in the form of strain increment is called plastic increment theory. Under the condition of proportional deformation, the constitutive relationship of the total quantity theory can be obtained through the constitutive relationship of integral increment theory. When the deviation from the proportional deformation condition is not much, the calculation result of the total quantity theory is close to the actual risk result.

Yield criterion, hardening rule and plastic flow rule are the three fundamental equations in plastic theory. Under complex stress conditions, yield criterion is useful to accurately determine the yielding of material. For isotropic materials like metals, while many yield criteria are available, the most commonly used yield conditions are the Tresca yield condition and Von Mises condition. However, the yield behavior of anisotropic materials like timber cannot be modelled by these yield criteria. Thus, the Hill anisotropic yield criterion was introduced by Hill in 1948 [21] as an anisotropic extension of the Von Mises criterion. The most of existing models for anisotropic materials are derived based on Hill's criterion which does not distinguish between compressive and tensile strengths. This can result in underestimation of the maximum load that can be applied. Thus, in this paper, a constitutive relationship is adopted for timber material based on the isotropic hardening elastoplastic model using the Hoffman yield criterion [23], which was introduced as an extension of Hill criterion considering the different tensile and compression strengths that could characterize the brittle behavior. The strength difference of timber in tension and compression can be considered for the description of the corresponding yield surface in the Hoffman theory. Compared to the material models based on Hill's criterion, in total nine independent material strength parameters representing three compressive strengths, three tensile strengths and three shear strengths of the material are necessary for the description of yield surface of the proposed material model for timber. In addition, in order to define linear-elastic orthotropic behavior of timber, a total of nine mechanical properties such as three elastic moduli, three shear moduli and three Poisson's ratios are used in the proposed material model.

In this paper, no plastic response is considered for the timber under tension and Hoffman criterion [23] is adopted to consider the plastic deformation of timber under compression. It means, the timber will show elastic response and will fail in a brittle way when it is subjected to tensile stress. If the timber is subjected to compression, once the stresses reaches the yield criterion, the timber will yield with plastic flow and hardening and will fail in a ductile way. The yield function $f(\sigma)$ used in this elastic–plastic model can be expressed by Eq. (10) [45].

$$f(\sigma) = \alpha_{23}(\sigma_2-\sigma_3)^2+\alpha_{13}(\sigma_3-\sigma_1)^2+\alpha_{12}(\sigma_1-\sigma_2)^2+\alpha_{11}\sigma_1+\alpha_{22}\sigma_2+\alpha_{33}\sigma_3+3\alpha_{44}\sigma_4^2+3\alpha_{55}\sigma_5^2+3\alpha_{66}\sigma_6^2-\sigma_e^2 \tag{10}$$

with

$$\alpha_{12} = \frac{\sigma_e^2}{2}\left(\frac{1}{\sigma_{1c}\sigma_{1t}}+\frac{1}{\sigma_{2c}\sigma_{2t}}-\frac{1}{\sigma_{3c}\sigma_{3t}}\right) \tag{11}$$

$$\alpha_{23} = \frac{\sigma_e^2}{2}\left(-\frac{1}{\sigma_{1c}\sigma_{1t}}+\frac{1}{\sigma_{2c}\sigma_{2t}}+\frac{1}{\sigma_{3c}\sigma_{3t}}\right) \tag{12}$$

$$\alpha_{13} = \frac{\sigma_e^2}{2}\left(\frac{1}{\sigma_{1c}\sigma_{1t}}-\frac{1}{\sigma_{2c}\sigma_{2t}}+\frac{1}{\sigma_{3c}\sigma_{3t}}\right) \tag{13}$$

$$\alpha_{11} = \sigma_e^2\left(\frac{\sigma_{1c}-\sigma_{1t}}{\sigma_{1c}\sigma_{1t}}\right) \tag{14}$$

$$\alpha_{22} = \sigma_e^2\left(\frac{\sigma_{2c}-\sigma_{2t}}{\sigma_{2c}\sigma_{2t}}\right) \tag{15}$$

$$\alpha_{33} = \sigma_e^2\left(\frac{\sigma_{3c}-\sigma_{3t}}{\sigma_{3c}\sigma_{3t}}\right) \tag{16}$$

$$\alpha_{44} = \frac{\sigma_e^2}{3\sigma_{12}^2} \tag{17}$$

$$\alpha_{55} = \frac{\sigma_e^2}{3\sigma_{13}^2} \tag{18}$$

$$\alpha_{66} = \frac{\sigma_e^2}{3\sigma_{23}^2} \tag{19}$$

where σ_1, σ_2 and σ_3 are the normal stresses in the direction of orthotropic axis *1*, *2* and *3*, respectively. σ_4, σ_5 and σ_6 are the shear stresses in the planes *12*, *13* and *23*, respectively. σ_e is the equivalent yield stress, σ_{ic} and σ_{it} ($i = 1, 2, 3$) are the compressive and tensile strengths in the axes of orthography, respectively. σ_{12}, σ_{13} and σ_{23} are the shear strengths in planes *12*, *13* and *23*, respectively.

The Hoffman yield criterion can be formulated as follows:

$$f(\sigma) = \frac{1}{2}\sigma^T P\sigma + \sigma^T Q - \sigma_e^2 \tag{20}$$

where, σ^T is the stress tensor in a vector form as $\sigma^T = (\sigma_1, \sigma_2, \sigma_3, \sigma_4, \sigma_5, \sigma_6)$. P and Q are the Hoffman mapping matrix and vector, respectively, defined in [45].

$$P = \begin{bmatrix} 2(\alpha_{13}+\alpha_{12}) & -2\alpha_{12} & -2\alpha_{13} & 0\ \ 0\ \ 0 \\ -2\alpha_{12} & 2(\alpha_{23}+\alpha_{12}) & -2\alpha_{23} & 0\ \ 0\ \ 0 \\ -2\alpha_{13} & -2\alpha_{23} & 2(\alpha_{13}+\alpha_{23}) & 0\ \ 0\ \ 0 \\ & 0\ \ 0\ \ 0 & & 6\alpha_{44}\ \ 0\ \ 0 \\ & 0\ \ 0\ \ 0 & & 0\ \ 6\alpha_{55}\ \ 0 \\ & 0\ \ 0\ \ 0 & & 0\ \ 0\ \ 6\alpha_{66} \end{bmatrix} \tag{21}$$

$$Q^T = (\alpha_{11},\ \alpha_{22},\ \alpha_{33},\ 0,\ 0,\ 0) \tag{22}$$

For an ideal elastoplastic material, since there is no strengthening effect, the value of the yield function remains constant during the entire plastic deformation process. For strengthened or softened materials, the yield condition will change with the increase of plastic deformation. The changed yield condition is called the subsequent yield condition. The proposed model considers linear isotropic hardening for timber yield stress under the compression as follows:

$$\sigma_{ek} = \sigma_e + h.k \tag{23}$$

where h is hardening modulus and k is the isotropic hardening variable.

k depends on the equivalent plastic strain obtained by means iterative method (Newton-Raphson) for each load increment. However, h is an input parameter of the proposed model which can be directly obtained from the uniaxial stress–strain diagram. Depending on the chosen value of h, perfect plasticity, slight hardening or softening can be modelled. Simply, the following equation can be used to calculate the value of h for a particular case of uniaxial plasticity [4].

$$h = \frac{\sigma_e}{\sigma_{2c}}\frac{E_2 T_2}{E_2 - T_2} \tag{24}$$

where T_2 is the plastic tangent modulus in the direction of orthotropic axis 2 (the direction perpendicular to the grain).

In the hardening state, each yield value will change depending on the corresponding hardening parameter k_i ($i = 1,2,..,9$). Thus, the parameters in the mapping vector Q change also. Isotropic hardening is considered in this paper, because it assumes that the initial yield surface expands uniformly without translation and distortion as plasticity occurs [46]. Thus, all the yield values change in the same order. Consequently, the parameters α_{11}, α_{22} and α_{33} in the mapping vector Q will change depending on the hardening parameter k. Thus, the Hoffman yield function combined with the isotropic hardening can be written in a general form as follows:

$$f(\sigma,k) = \frac{1}{2}\sigma^T P\sigma + \sigma^T Q(k) - \sigma_{ek}^2 \tag{25}$$

The stress point must remain on the yield surface to obtain plastic deformations. The yield condition is the condition that each combination of stress components should satisfy. Mathematically speaking, the yield function must be less than zero for elastic deformations and it must remain zero for a short period for material yielding so that plastic flow can occur.

$$f(\sigma,k) < 0 \quad \text{for elastic} \tag{26}$$

$$f(\sigma,k) = 0 \quad \text{yield condition} \tag{27}$$

When the stress reaches the strength criterion of Eq. (27), the elastoplastic radial mapping algorithm is used to constrain stress point on the yield surface. According to the theory of plasticity, the total strain increment $\Delta\varepsilon$ can be divided into elastic component $\Delta\varepsilon^e$ and plastic component $\Delta\varepsilon^p$ as:

$$\Delta\varepsilon = \Delta\varepsilon^e + \Delta\varepsilon^p \tag{28}$$

In this study, the associated flow rule was used to determine the plastic strain and is given as:

$$\Delta\varepsilon^p = \Delta\lambda\left(\frac{\partial f}{\partial\sigma}\right) \tag{29}$$

where $\Delta\lambda$ denotes the plastic multiplier and $\frac{\partial f}{\partial\sigma}$ is the gradient vector of the plastic potential energy function of $f(\sigma,k)$ which can be written as:

$$\left(\frac{\partial f}{\partial \sigma}\right) = \begin{pmatrix} 2(\alpha_{13}+\alpha_{12})\sigma_1 - 2\alpha_{12}\sigma_2 - 2\alpha_{13}\sigma_3 + \alpha_{11} \\ -2\alpha_{12}\sigma_1 + 2(\alpha_{23}+\alpha_{12})\sigma_2 - 2\alpha_{23}\sigma_3 + \alpha_{22} \\ -2\alpha_{13}\sigma_1 - 2\alpha_{23}\sigma_2 + 2(\alpha_{13}+\alpha_{23})\sigma_3 + \alpha_{33} \\ 6\alpha_{44}\sigma_4 \\ 6\alpha_{55}\sigma_5 \\ 6\alpha_{66}\sigma_6 \end{pmatrix} \tag{30}$$

2.3. Damage evolution equations

A damage model is needed to characterise the different responses of timber in tension and compression. The damage in any direction of the timber causes a gradual degradation of its stiffness. The effective stress concept has been successfully used in the most damage mechanics models recently. The effective stress is the stress acting on the undamaged material. According to the continuum damage mechanics, the hypothesis of strain equivalence states that the strain associated with the Cauchy stress in the damaged state is equivalent to the strain associated with the effective stress in the undamaged state [47]. Therefore, the relationship of the Cauchy stress, that is the stress tensor associated with the damaged state, σ, and the effective stress tensor associated with the undamaged state, $\overline{\sigma}$, can be described by the following equation:

$$\sigma = M(d)\overline{\sigma} \tag{31}$$

where $M(d)$ is a fourth-order tensor which characterise the state of damage.

Accordingly, the constitutive relationships of undamaged and damaged states of timber, respectively, are given as

$$\overline{\sigma} = E\varepsilon_e \tag{32}$$

$$\sigma = E_d\varepsilon_e \tag{33}$$

where E_d is the damaged stiffness matrix.

In this study, anisotropic damage with non-uniform distribution of micro cracks and voids in all directions of the timber matrix is considered. To consider the anisotropic damage, three different damage factors must be introduced. The reduction of the elastic stiffness matrix is simulated here as a function of damage evolution in three orthogonal directions. Therefore, the damaged stiffness matrix with the damage factors can be written as [48]

$$E_d = \begin{bmatrix} (1-d_1)E_{11} & (1-d_1)(1-d_2)E_{12} & (1-d_1)(1-d_3)E_{13} & 0 & 0 & 0 \\ (1-d_1)(1-d_2)E_{12} & ((1-d_2)E_{22} & (1-d_2)(1-d_3)E_{23} & 0 & 0 & 0 \\ (1-d_1)(1-d_3)E_{13} & (1-d_2)(1-d_3)E_{23} & (1-d_3)E_{33} & 0 & 0 & 0 \\ 0 & 0 & 0 & (1-d_1)(1-d_2)E_{44} & 0 & 0 \\ 0 & 0 & 0 & 0 & (1-d_1)(1-d_3)E_{55} & 0 \\ 0 & 0 & 0 & 0 & 0 & (1-d_2)(1-d_3)E_{66} \end{bmatrix} \tag{34}$$

where d_1, d_2 and d_3 are the damage factors defined in the longitudinal, radial and tangential directions, respectively. The damage factor, d_i ($i = 1,2,3$), increases from 0 to 1 as damage grows from threshold value to its ultimate value.

Since the timber has different damage evolution for tensile and compression failures, the damage models proposed by Wang et al. [49] are used to define the tensile and compression damage evolutions. In this study, different tensile damages in three orthogonal directions and compressive damage in only longitudinal direction were considered as shown in Eqs. (35) and (36).

$$d_{it} = 1 - \frac{1}{F_{it}} e^{\left((1-F_{it})\frac{L_c\sigma_{it}^2}{E_i G_{it}^f}\right)} \quad (i = 1,2,3) \tag{35}$$

$$d_{1c} = 1 - \frac{1}{F_{1c}}(1-A) - Ae^{B(1-F_{1c})} \tag{36}$$

where d_{it}, and G_{it}^f are the tensile damage factor and fracture energy under tension in the i-th direction of the timber, respectively. d_{1c} is the compression damage factor in the longitudinal direction of the timber. L_c is the element characteristic length. F_{it} and F_{1c} are the variables defined in Eqs. (35) to (38). A and B are the material constants.

The stress-based continuum damage formulation with different failure criteria in tension and compression is used in this study. It means, damage starts to accumulate as soon as the stresses satisfy the failure criterion. The failure criterion proposed by Sandhaas and Van de Kuilen [34] is used in this study due to successful applications in combining ductile and brittle failures within on model, which is described as

$$If\ \ \sigma_1 < 0; \quad F_{1c} = \frac{-\sigma_1}{\sigma_{1c}} \le 1 \tag{37}$$

$$If\ \ \sigma_1 > 0;\quad F_{1t} = \frac{\sigma_1}{\sigma_{1t}} \le 1 \tag{38}$$

$$If\ \ \sigma_2 > 0;\quad F_{2t} = \left(\frac{\sigma_2}{\sigma_{2t}}\right)^2 + \left(\frac{\sigma_4}{\sigma_{12}}\right)^2 + \left(\frac{\sigma_6}{\sigma_{23}}\right)^2 \le 1 \tag{39}$$

$$If\ \ \sigma_3 > 0;\quad F_{3t} = \left(\frac{\sigma_3}{\sigma_{3t}}\right)^2 + \left(\frac{\sigma_5}{\sigma_{13}}\right)^2 + \left(\frac{\sigma_6}{\sigma_{23}}\right)^2 \le 1 \tag{40}$$

Damage models can encounter convergence problems in static analysis. In order to improve the convergence, viscous regularisation method [50,51] is used to define the model. In the viscous regularisation, the response of damaged material is evaluated using a viscous regularised damage variable d^v which is defined as

$$\dot{d}^v = \frac{1}{\eta}(d - d^v) \tag{41}$$

where η is the viscous parameter. A small value of the viscous parameter usually helps to improve the convergence rate of the model without significantly influencing the results. Thus, the value of viscous parameter is chosen to be equal to 0.0001, in this study.

By the introduction of Δt, that is the increment of time, into Eq. (41), the regularised damage variable at the $(n+1)^{\text{th}}$ load increment can be derived as

$$d^v_{n+1} = \frac{\eta}{\eta + \Delta t} d^v_n + \frac{\Delta t}{\eta + \Delta t} d_{n+1} \tag{42}$$

where d^v_n and d^v_{n+1} are the regularised damage variables of the n^{th} and $(n+1)^{\text{th}}$ steps, respectively. d_{n+1} is the non-regularised damage variable of the $(n+1)^{\text{th}}$ step.

2.4. Numerical integration

In the numerical algorithm, nonlinear plastic response of timber, as elastoplastic orthotropic material under three-dimensional (3D) stress state, is solved by the use of strain increment-based method. The numerical integration steps are presented in this section.

At the moment t_{n+1}, the state variables ε_n, ε^e_n, ε^p_n, $\Delta\varepsilon_{n+1}$, σ_n, $\sigma_{ek,n}$, and $d_{i,n}$ are known. The current value of the total strain ε_{n+1} can be expressed as

$$\varepsilon_{n+1} = \varepsilon_n + \Delta\varepsilon_{n+1} \tag{43}$$

The effective stress at the end of the load increment $n + 1$, $\overline{\sigma}_{n+1}$, can be calculated as a summation of the effective stress at the beginning of the load increment $\overline{\sigma}_n$and the stress increment $\Delta\overline{\sigma}_{n+1}$.

$$\overline{\sigma}_{n+1} = \overline{\sigma}_n + \Delta\overline{\sigma}_{n+1} \tag{44}$$

Substitution of Eq. (33) into Eq. (44) and rearranging gives

$$\overline{\sigma}_{n+1} = \overline{\sigma}_n + E\Delta\varepsilon^e_{n+1} \tag{45}$$

According to the theory of plasticity, for the finite load increment $n + 1$, the increment of total strain $\Delta\varepsilon_{n+1}$ can be divided into an elastic component $\Delta\varepsilon^e_{n+1}$ and a plastic component $\Delta\varepsilon^p_{n+1}$.

$$\Delta\varepsilon_{n+1} = \Delta\varepsilon^e_{n+1} + \Delta\varepsilon^p_{n+1} \tag{46}$$

Therefore, subsequent substitution of Eq. (46) into Eq. (45) and rearranging gives

$$\overline{\sigma}_{n+1} = \overline{\sigma}_n + E(\Delta\varepsilon_{n+1} - \Delta\varepsilon^p_{n+1}) \tag{47}$$

In the developed algorithm, an elastic predictor step is carried out to predict the trial elastic stress $\overline{\sigma}^{trial}_{n+1}$ considering no plastic strain increment in the $n + 1$ load increment as

$$\overline{\sigma}^{trial}_{n+1} = \overline{\sigma}_n + E\Delta\varepsilon_{n+1} \tag{48}$$

Then, by the substitution of Eq. (44) into Eq. (43), the plastic corrector of the effective stress in the $n + 1$ load increment can be derived as

$$\overline{\sigma}_{n+1} = \overline{\sigma}^{trial}_{n+1} - E\Delta\varepsilon^p_{n+1} \tag{49}$$

The incremental plastic strain $\Delta\varepsilon^p_{n+1}$can be written as the product of a plastic multiplier $\Delta\lambda$ and the derivative of $f(\overline{\sigma},k)$ with respect to $\overline{\sigma}$.

$$\Delta\varepsilon^p_{n+1} = \Delta\lambda_{n+1}\left(\frac{\partial f}{\partial \overline{\sigma}}\right)_{n+1} \tag{50}$$

where

$$\left(\frac{\partial f}{\partial \overline{\sigma}}\right)_{n+1} = \begin{pmatrix} 2(\alpha_{13}+\alpha_{12})\sigma_1 - 2\alpha_{12}\sigma_2 - 2\alpha_{13}\sigma_3 + \alpha_{11} \\ -2\alpha_{12}\sigma_1 + 2(\alpha_{23}+\alpha_{12})\sigma_2 - 2\alpha_{23}\sigma_3 + \alpha_{22} \\ -2\alpha_{13}\sigma_1 - 2\alpha_{23}\sigma_2 + 2(\alpha_{13}+\alpha_{23})\sigma_3 + \alpha_{33} \\ 6\alpha_{44}\sigma_4 \\ 6\alpha_{55}\sigma_5 \\ 6\alpha_{66}\sigma_6 \end{pmatrix}_{n+1} \tag{51}$$

It can also be written as

$$\left(\frac{\partial \mathrm{f}}{\partial \overline{\sigma}}\right)_{\mathrm{n+1}} = \mathrm{P}\overline{\sigma}_{\mathrm{n+1}} + \mathrm{Q}_{n+1} \tag{52}$$

Subsequent substitution of Eqs. (50) and (52) Eq. (49) and rearranging gives

$$\overline{\sigma}_{n+1} = \overline{\sigma}^{trial}_{n+1} - E\Delta\lambda_{n+1}(P\overline{\sigma}_{\mathrm{n+1}} + \mathrm{Q}_{n+1}) \tag{53}$$

According to Owen and Hinton [52], the incremental equivalent plastic strain $\Delta\overline{\varepsilon}^p$can be defined as,

$$\Delta\overline{\varepsilon}^p = \sqrt{\frac{2}{3}(\Delta\varepsilon^p)^T Z\Delta\varepsilon^p} \tag{54}$$

with

$$Z = \begin{bmatrix} 1 & 0 & 0 & 0 & 0 & 0 \\ 0 & 1 & 0 & 0 & 0 & 0 \\ 0 & 0 & 1 & 0 & 0 & 0 \\ 0 & 0 & 0 & 0.5 & 0 & 0 \\ 0 & 0 & 0 & 0 & 0.5 & 0 \\ 0 & 0 & 0 & 0 & 0 & 0.5 \end{bmatrix} \tag{55}$$

Now Eq. (54) can be rewritten with the aid of Eqs. (50) and (52) as follows:

$$\Delta\overline{\varepsilon}^p{}_{n+1} = \Delta\lambda_{n+1}\sqrt{\frac{2}{3}\left(\frac{\partial \mathrm{f}}{\partial \overline{\sigma}}\right)^T_{n+1} Z\left(\frac{\partial \mathrm{f}}{\partial \overline{\sigma}}\right)_{\mathrm{n+1}}} \tag{56}$$

$$\Delta\overline{\varepsilon}^p{}_{n+1} = \Delta\lambda_{n+1}\sqrt{\frac{2}{3}\left(\mathrm{P}\overline{\sigma}_{\mathrm{n+1}} + \mathrm{Q}_{n+1}\right)^T Z(\mathrm{P}\overline{\sigma}_{\mathrm{n+1}} + \mathrm{Q}_{n+1})} \tag{57}$$

$$\overline{\varepsilon}^p{}_{n+1} = \overline{\varepsilon}^p{}_n + \Delta\lambda_{n+1}\sqrt{\frac{2}{3}\left(\mathrm{P}\overline{\sigma}_{\mathrm{n+1}} + \mathrm{Q}_{n+1}\right)^T Z(\mathrm{P}\overline{\sigma}_{\mathrm{n+1}} + \mathrm{Q}_{n+1})} \tag{58}$$

where $\overline{\varepsilon}^p{}_n$ and $\overline{\varepsilon}^p{}_{n+1}$ are the equivalent plastic strain at the beginning and at the end of the load step increment, respectively.

According to the Eqs. (53) and (58), the updated effective stress $\overline{\sigma}_{n+1}$and equivalent plastic strain $\overline{\varepsilon}^p{}_{n+1}$ are a function of $\Delta\lambda$. The Newton-Raphson method is used to obtain the unknown parameter $\Delta\lambda_{n+1}$. At the end of $n+1$ load increment, the updated stresses and effective accumulated plastic strain must also satisfy the yield criterion condition. Then, Eq. (25) gives:

$$f_{n+1} = \frac{1}{2}\overline{\sigma}^T_{n+1}P\overline{\sigma}_{n+1} + \overline{\sigma}^T_{n+1}Q_{n+1} - \left(\sigma^2_{ek}\right)_{n+1} = 0 \tag{59}$$

In the Newton-Raphson method, if $\Delta\lambda$ has approximate expression $f(\Delta\lambda) = 0$ is not true, there are residual values. In fact, in specific calculations, when $f(\Delta\lambda) \neq 0$, but extremely small (less than 10^{-9}), then it is considered that f is close to the true value and the iteration is stopped. In this method, the k^{th} iteration of the $\Delta\lambda$ is obtained as,

$$\Delta\lambda^k = \Delta\lambda^{k-1} + \delta\Delta\lambda^k \tag{60}$$

If the k^{th} iteration is a true solution, it can be expanded according to the Taylor series as,

$$f(\Delta\lambda)^k = f(\Delta\lambda)^{k-1} + \left(\frac{df(\Delta\lambda)}{d\Delta\lambda}\right)^{k-1}\delta\Delta\lambda^k = 0 \tag{61}$$

Then,

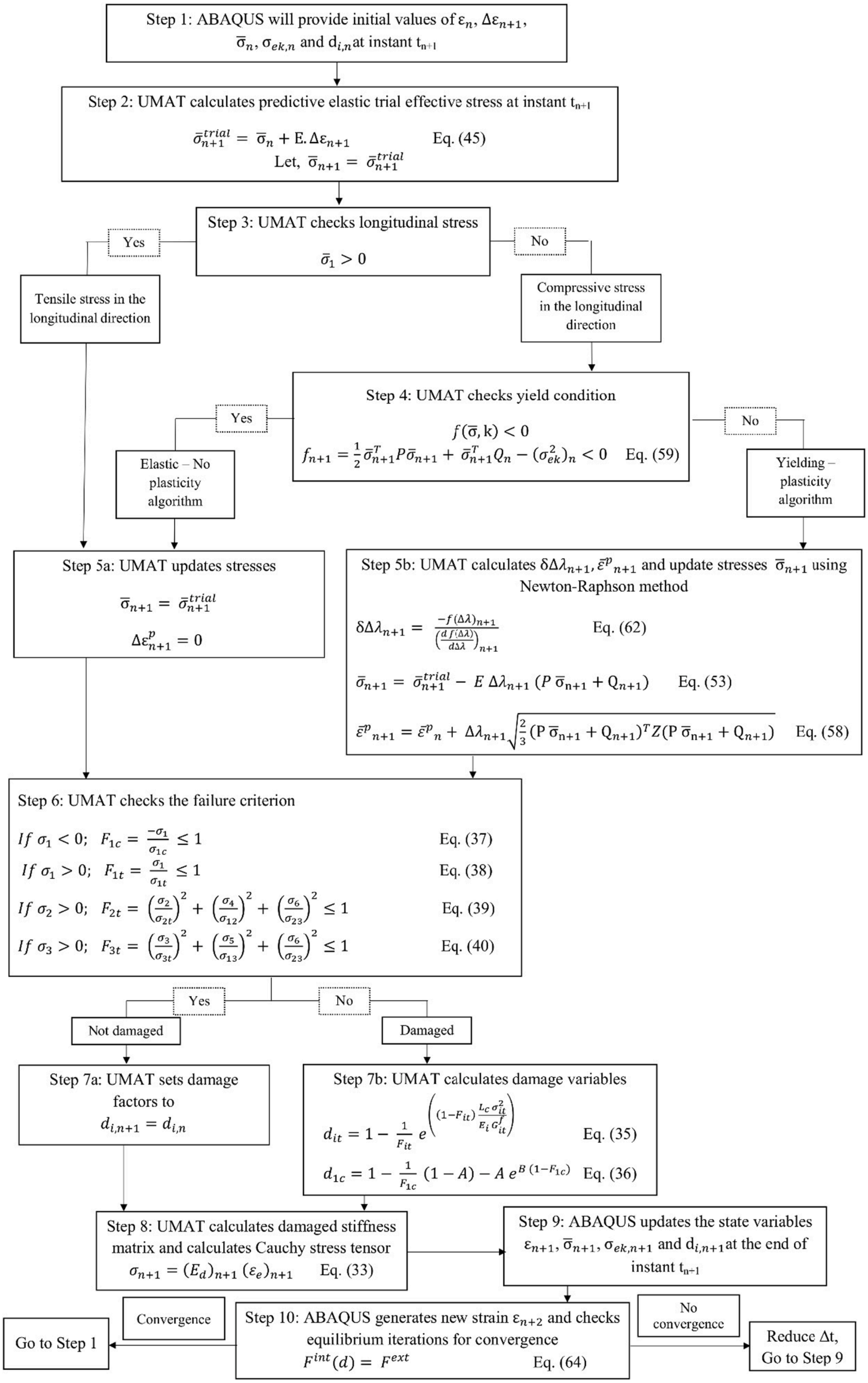

Fig. 1. Flow chart for analysis of timber material in UMAT.

$$\delta\Delta\lambda^{k} = \frac{-f(\Delta\lambda)^{k-1}}{\left(\frac{df(\Delta\lambda)}{d\Delta\lambda}\right)^{k-1}} \tag{62}$$

The derivative of f is given by

$$\frac{df(\Delta\lambda)}{d\Delta\lambda} = (P\overline{\sigma} + Q)\frac{d\overline{\sigma}}{d\Delta\lambda} - 2\sigma_e\frac{d\overline{\sigma}}{d\overline{\varepsilon}^p}\frac{d\overline{\varepsilon}^p}{d\Delta\lambda} \tag{63}$$

When $\Delta\lambda$ is computed, the new stress $\overline{\sigma}_{n+1}$ and equivalent plastic strain $\overline{\varepsilon}^{p}{}_{n+1}$ can be computed using Eqs. (53) and (58), respectively. Subsequently, plastic strain ε^p_{n+1} and elastic strain ε^e_{n+1} will be updated. Then, the damage factors and damaged stiffness matrix are computed using Eqs. (34) to (36). Accordingly, the final stress σ_{n+1} at the end of load increment $n+1$ can be updated using Eq. (33).

3. UMAT implementation in ABAQUS

Today vast number of Finite Element (FE) codes are available that are capable of analyzing challenging engineering problems. Among many finite element analysis software, researchers are keen to use ABAQUS because it provides users with powerful, easy-to-use secondary development tools and interfaces, allowing users to easily carry out FE modelling, analysis and post-processing to meet the needs of specific engineering problems. Through the user material subroutine interface, the user can define any supplementary material model.

This research work aims to develop a user subroutine for the timber material model. As described in the previous chapter, the constitutive relationship adopted in this paper is the isotropic hardening elastoplastic model coupled with the Hoffman yield criterion and anisotropic damage. The implicit integration algorithm formulas for calculating the problem are derived from the Newton-Raphson method. The ABAQUS/Standard FE software was used to conduct numerical simulations via a Fortran UMAT user subroutine. The flow diagram of the developed timber material subroutine is shown in Fig. 1.

To implement the previously described material law a user-defined material model (UMAT) was implemented as a subroutine in ABAQUS. Regarding the writing format of UMAT, the variables commonly used in UMAT are defined at the beginning of the file. As described in the previous chapter, in addition to the typical nine orthotropic elasticity parameters, the proposed material model requires three compressive strengths, three tensile strengths and three shear strengths parameters as well as two strain hardening parameters, which leads to a total of twenty input parameters.

In the code, for a given strain increment $\Delta\varepsilon_{n+1}$ (DSTRAN), the results of the previous time step t_n, that is stress σ_n and strain ε_n, are used to calculate and update the Jacobian matrix (DDSDDE), stress tensor (STRESS) and solution-dependent state variables (STATEV) at the current time step t_{n+1}. First, the trial stress is calculated using the elastic stiffness matrix. Then, if the longitudinal stress is compressive, it is evaluated in order to determine if there is strain-hardening or not. In the next step, the compression stress is evaluated into the flow criterion is derived from Hoffman yield function coupled with the strain hardening is described by the effective plastic strain to transfer the yield surface. In the case of plasticity, the value of plastic multiplier $\Delta\lambda_{n+1}$ and the equivalent plastic strain $\overline{\varepsilon}^{p}{}_{n+1}$ are obtained by solving the equations above according to the Newton-Raphson method. In the next step, the effective stress tensor and the stiffness matrix are updated. In the case of no plasticity, the effective stress tensor is updated with the trial stress. Then, the conditions of the failure criterion is evaluated and the damage variables are calculated. Following, the effective stress tensor and the Jacobian matrix are updated. At the end of UMAT, the updated value of the variable will be returned to the ABAQUS solver through the interface and convergence conditions must be satisfied.

In ABAQUS implicit analysis, the displacement of the node (and thus the strain) is calculated, so that the balance of internal force and external force is as follows:

$$F^{int}(d) = F^{ext} \tag{64}$$

where d is the vector of displacement of nodes, and F^{int} and F^{ext} are the internal force vector and external force vector, respectively. Except for small deformation and linear elasticity problems, Eq. (64) is non-functional, and an iterative method should be used to solve the discretized equilibrium equation for the FE model as follows:

$$F^{ext}_{n+1} - F^{int}\left(d^i_{n+1}\right) = K_T\Delta d \tag{65}$$

$$d^{i+1}_{n+1} = d^i_{n+1} + \Delta d \tag{66}$$

where K_T is the global tangent stiffness matrix, i represents the ith iteration within an incremental step, and n represents the nth incremental step.

Iterations are repeated in each time increment until convergence is achieved. To converge quickly, the displacement increment should change along the direction of the gradient. No matter how fast the convergence is, the Eq. (64) for force equilibrium which is attained at every node, is the only criterion for judging the accuracy of the results.

4. Results and discussion

In this section, the performance and accuracy of the developed model are verified against an experimental test and some examples

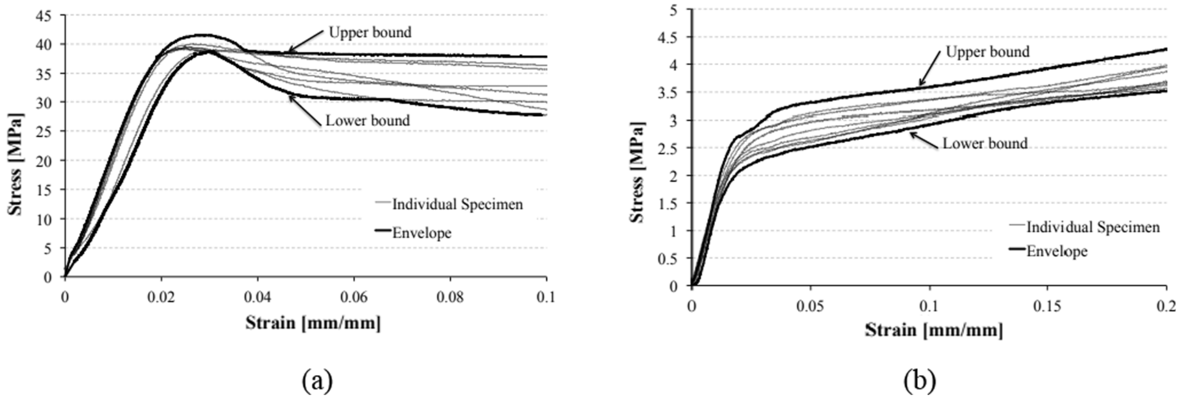

Fig. 2. Stress–strain relationships from compression tests (a) parallel (b) perpendicular to the grain [53].

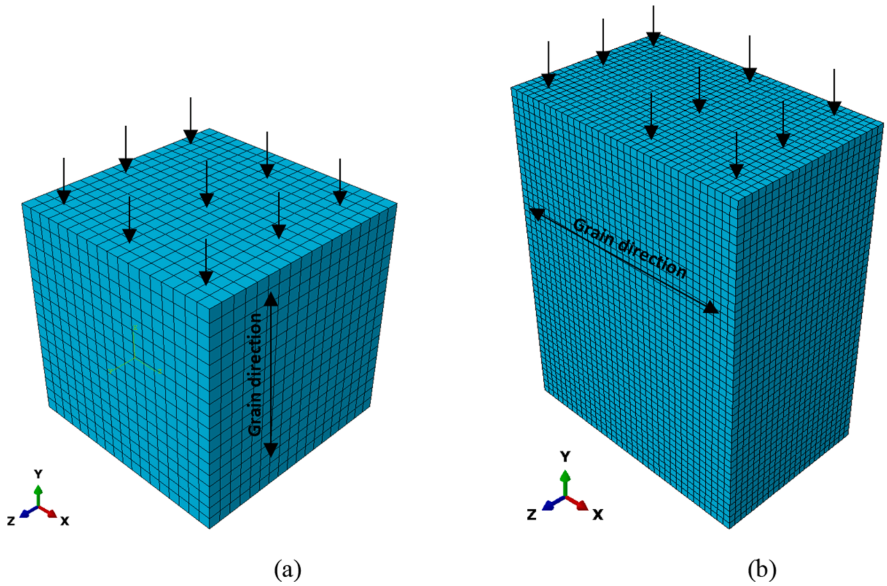

Fig. 3. FE models for uniaxial compression tests (a) parallel (b) perpendicular to the grain.

obtained by other researchers. A timber specimen under 4-point bending is simulated in the first simulation to validate the timber model introduced in this paper in predicting the flexural behavior of timber. Compressive tests for parallel to grain and perpendicular to grain which are conducted by Kargiannis et al. [53] and Oudejene and Khelifa [24] are simulated in the second example to validate the proposed material model in compression. In the third example, the tensile test results presented in ref. [37] are used to validate the timber model in tension.

4.1. Example 1: Compression test

Several authors have described that timber depicts a compressive failure with softening parallel to grain while the loading in the perpendicular direction to the grain exhibits a plateau region due to the plastic yielding and the damage evolution, after the linear elastic response [3,24,53,54,28]. Hence, in this example, the developed material model for timber is examined for the compression and verified against the available test data in refs. [24,53]. The compressive strength of a material is the capacity of a material to withstand loads tending to reduce size. The compressive strengths of the timber vary along the grain and against the grain. Thus, the compression behavior of timber with loads acting parallel and perpendicular to the grain are studied in this example. Karagiannis et al. [53] conducted a series of compression and shear load tests using Scandinavian spruce specimens with a mean density of 430 kg/m^3 and a moisture content of approximately 10%, according to European standards EN408. In order to validate the developed material model under uniaxial compressive loadings, compressive test results from Karagiannis et al. [53] was chosen in this study. For the compression tests, they have used a total of eight wood cubes of 45 mm × 45 mm × 45 mm and nine wood cuboids of 45 mm × 70 mm × 90 mm under compression parallel and perpendicular to the grain direction, respectively. The axial load was incrementally increased

Table 1
Material properties of wood for FE modelling of compression tests.

Elasticity parameters					
E_1 (MPa)	$E_2 = E_3$ (MPa)	G_{23} (MPa)	$G_{12} = G_{13}$ (MPa)	υ_{23}	$\upsilon_{12} = \upsilon_{13}$
2050.8	172.1	68	145.2	0.5	0.45
Strength components					
σ_{1c} (MPa)	$\sigma_{2c} = \sigma_{3c}$ (MPa)	σ_{1t} (MPa)	$\sigma_{2t} = \sigma_{3t}$ (MPa)	σ_{23} (MPa)	$\sigma_{12} = \sigma_{13}$ (MPa)
35	2.5	20	0.7	0.5	5
Hardening parameters					
h (MPa)					
1200					
Fracture energies					
$G_{1t,f}$ (N/mm)	$G_{2t,f}$ (N/mm)	$G_{3t,f}$ (N/mm)			
60	0.5	0.5			

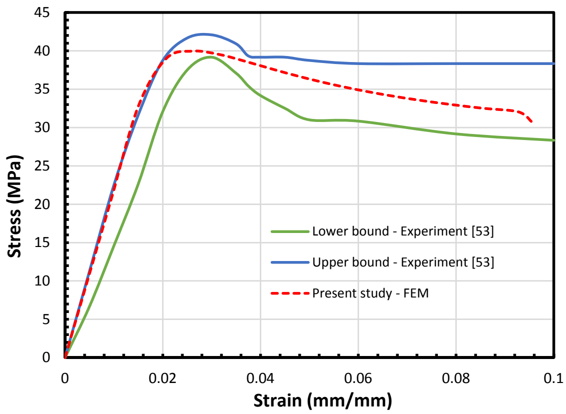

(a)

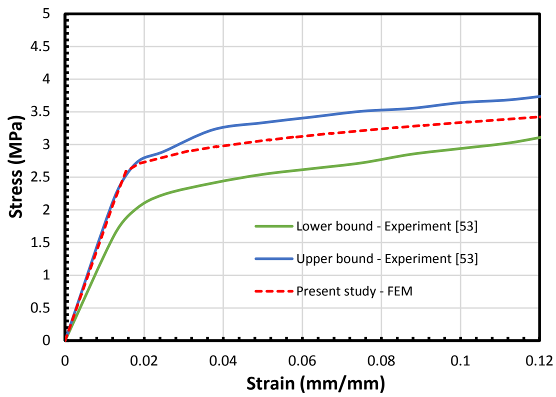

(b)

Fig. 4. Stress versus strain curves for uniaxial compression tests (a) parallel (b) perpendicular to the grain.

at a rate of 1 mm/min. Fig. 2 shows the obtained curves of the stress versus the strain for the compressions tests [53].

Fig. 3 shows the FE models used for the numerical simulations to adequately reproduce the uniaxial compression tests carried out on these real specimens of Karagiannis et al. [53]. Eight-node 3D elements (C3D8R) were used to discretize the timber cube and cuboid. The bottom of the wood specimens was assumed to be fixed in all directions. The simulations were carried out by applying a downward load acting on the top surface of the specimens. The material properties adopted for wood are listed in Table 1.

The stress–strain curves obtained from the numerical analyses are selected to compare the numerical results with the experimental results. Fig. 4(a) illustrates the obtained stress–strain curve from the numerical analysis until the failure under loading parallel to the grain. It can be seen that under compression parallel to the grain, the timber cube shows an almost linear elastic behavior until the compression strength of timber, and then shows a plastic behavior as observed by Karagiannis et al. [53]. As the predicted stress–strain curve ranges between the upper and lower bound of the experimental results, it can be stated that the FE model predicts the stress–strain curve with good agreement compared to experimental results [53].

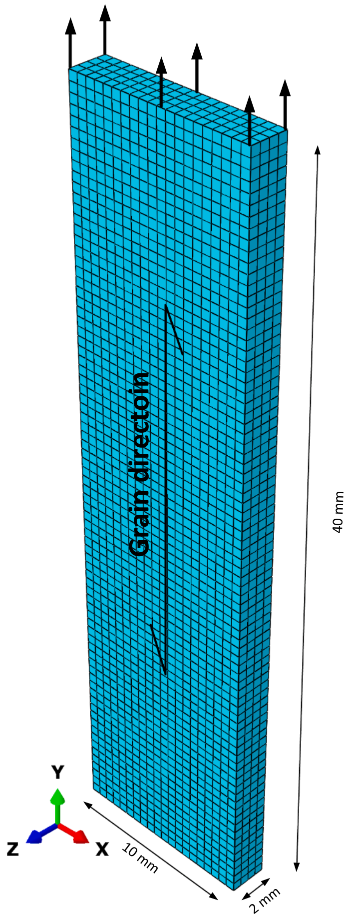

Fig. 5. FE model for uniaxial tensile test.

Table 2
Material properties of timber for FE modelling.

Elasticity parameters					
E_1 (MPa)	$E_2 = E_3$ (MPa)	G_{23} (MPa)	$G_{12} = G_{13}$ (MPa)	υ_{23}	$\upsilon_{12} = \upsilon_{13}$
13,010	870	340	980	0.02	0.29
Strength components					
σ_{1c} (MPa)	$\sigma_{2c} = \sigma_{3c}$ (MPa)	σ_{1t} (MPa)	$\sigma_{2t} = \sigma_{3t}$ (MPa)	σ_{23} (MPa)	$\sigma_{12} = \sigma_{13}$ (MPa)
50	4.5	43.1	0.7	0.5	6.9
Fracture energies					
$G_{1t,f}$ (N/mm)	$G_{2t,f}$ (N/mm)	$G_{3t,f}$ (N/mm)			
5	0.7	0.7			

The results obtained under loading perpendicular to the grain are shown in Fig. 4(b). It is also observed that the predicted stress–strain curve has a good correlation with the experimental curve as again the numerical results range between the upper and lower bound of the experimental results. Although the results of the experiment varies, the trends of the graphs are similar. Timber shows a linear elastic behavior and plastic hardening under the compression perpendicular to the grain. A good level of agreement between the numerically predicted stress–strain curve and their corresponding experimental results under both compression tests, the tests parallel and perpendicular to the grain, demonstrate that the proposed material model adequately simulates the non-linear response of the timber element in compression.

4.2. Example 2: Tensile test

In this part, the developed material model for timber is validated under tensile stress in comparison to the available experimental data [37] found in literature. Khennane et al. [37] developed a numerical model for the failure of timber under bending and tension

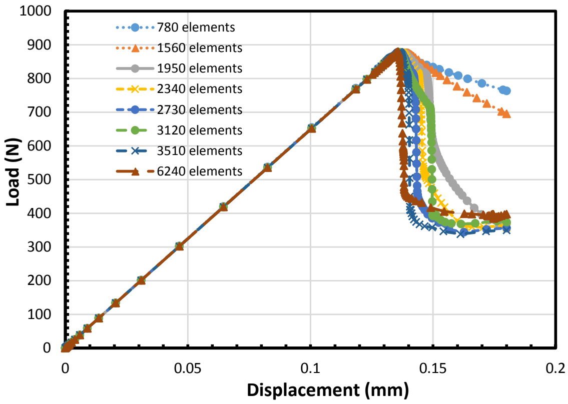

Fig. 6. Load-displacement from numerical study with different mesh sizes.

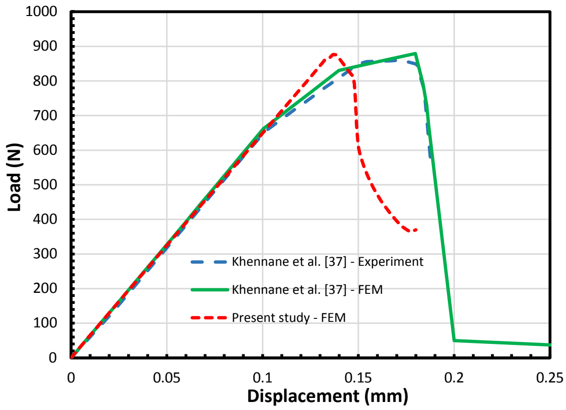

Fig. 7. Load-displacement curves of timber under uniaxial tension force.

parallel to the grain direction and compared the result of the material model to experimental results. In this example, the results of uniaxial tensile modelling is compared to the results from Khennane et al. [37].

Khennane et al. [37] conducted the tensile tests using 40 mm long × 10 mm wide × 2 mm thick pine wood specimen with the density of 460 kg/m^3. The tensile test parallel to the gain direction was carried out and the axial load was incrementally increased at a rate of 1 mm/min. A rectangular cuboid timber specimen with the dimensions of 40 mm × 10 mm × 2 mm was modelled with the material model developed in this study under the uniaxial tensile test as depicted in Fig. 5. Since strain hardening is not considered for timber under tension, the hardening modulus is not important for the analysis. The same modelling procedure that has been used in two previous examples is used here as well. The properties of the timber that were used as the inputs of the UMAT are shown in Table 2. The specimen was meshed using the C3D8R element available in ABAQUS/Standard library. Fixed boundary conditions were applied at the two ends of the specimen and the loading was implemented by displacement in the Y-direction parallel to the grain.

The FE model mesh size influences significantly on the behavior of the model when the material exhibits softening. This is due to the energy dissipation decreases with the mesh refinement. Therefore, a mesh sensitivity study was carried out with 780, 1560, 1950, 2340, 2730, 3120, 3510 and 6240 elements. The load–displacement curves of the numerical results for each case are shown in Fig. 6. It is evident that the softening stage of material is strongly dependent on the mesh size. However, it is also clear that the models with finer meshes have considerably similar softening behavior of the material.

To validate the model, the load–displacement diagram of the numerical and the experimental results are compared in Fig. 7. The results from the load–displacement curve of the FE model show satisfactory compatibility with the experimental results from Khennane et al. [37]. It can be seen that the specimen starts to deform linearly before reaching the yield strength and the model accurately predicts the brittle failure of timber specimen under tension. Even though the failure strain was underestimated, the model predicts the characteristic tensile strength of timber and failure mode precisely. As mentioned above, the differences in results are caused by the differences in actual timber specimens and material properties used in the numerical model.

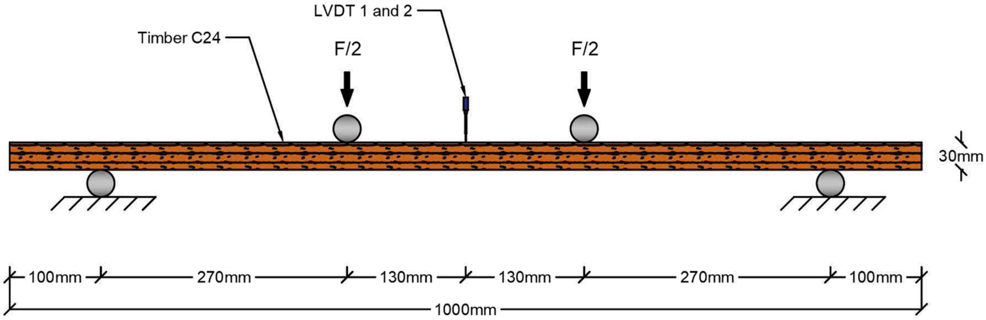

Fig. 8. Experimental Setup.

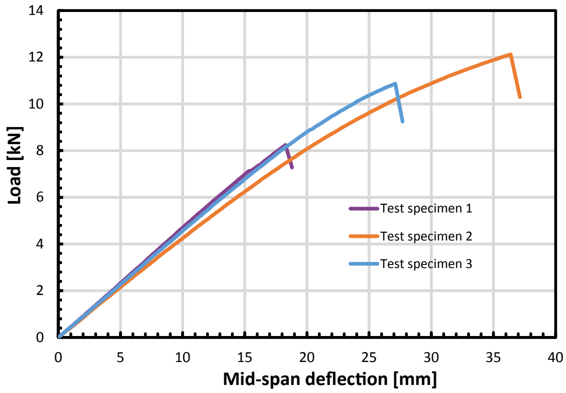

Fig. 9. Load-deformation curves of the test specimens.

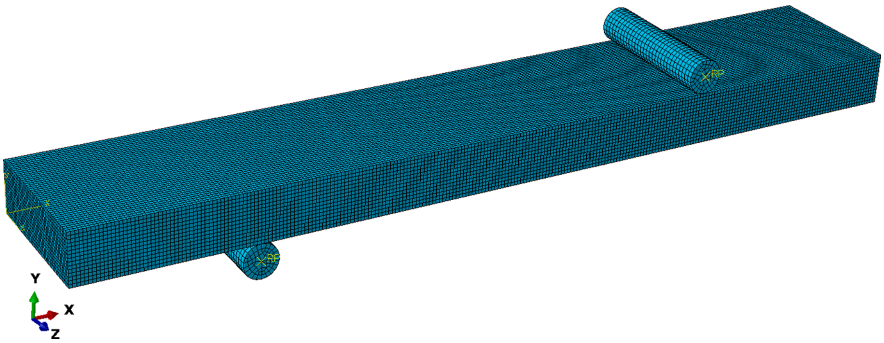

Fig. 10. Quarter of FE model of a four-point bending test.

4.3. Example 3: Bending test

In this section, to validate the constitutive timber model under bending two models have been developed. In both models, timber is modelled as elastoplastic orthotropic material according to Hoffman yield criterion coupled with isotropic hardening. However, the anisotropic damage evolution combined with the failure criterion is not used in first model (Model 1). In second model (Model 2), the damage evolution combined with the failure criterion proposed by Sandhaas and Van de Kuilen [34], discussed in Section 2.3, is associated with Hoffmann yield criterion is adopted to model the timber.

To validate the model, the experimental test program carried out by the authors at the laboratory of Solid Structures of the University of Luxembourg is used. Three timber boards manufactured from KVH-Si timber material of strength class C24 were tested under four-point bending tests. The specimens of length 1 m had a cross section of 30 mm × 170 mm. All the timber boards were simply supported over 0.8 m span and they were subjected to two-point loading through two 30 mm diameter steel rods which were positioned at a distance of 0.37 m from the ends of the timber board, as shown in Fig. 8. The loads were applied at a loading rate of 0.1 kN/

Table 3
Material properties of timber for FE modelling.

Elasticity parameters					
E_1 (MPa)	$E_2 = E_3$ (MPa)	G_{23} (MPa)	$G_{12} = G_{13}$ (MPa)	υ_{23}	$\upsilon_{12} = \upsilon_{13}$
11,000	370	60	690	0.5	0.45
Strength components					
σ_{1c} (MPa)	$\sigma_{2c} = \sigma_{3c}$ (MPa)	σ_{1t} (MPa)	$\sigma_{2t} = \sigma_{3t}$ (MPa)	σ_{23} (MPa)	$\sigma_{12} = \sigma_{13}$ (MPa)
36	4.6	24	0.7	0.5	6.9
Hardening parameters					
h (MPa)					
6436					
Fracture energies					
$G_{1t,f}$ (N/mm)	$G_{2t,f}$ (N/mm)	$G_{3t,f}$ (N/mm)			
6	0.5	0.5			

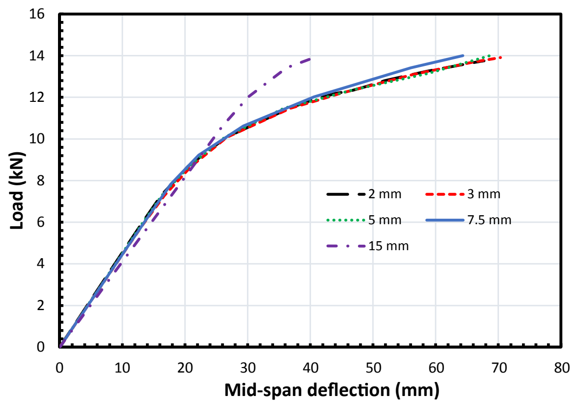

Fig. 11. Load vs mid-span deflection for various meshing size.

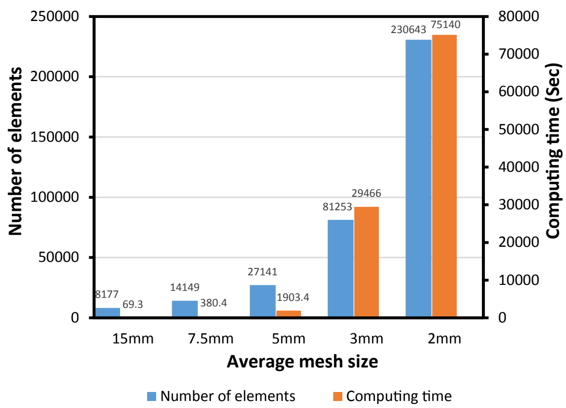

Fig. 12. Computing time vs number of elements for various mesh size.

s. During the experiment, mid-span deflection of the timber board was measured a LVDT (Linear Variable Displacement Transducer) mounted on the top face of the specimen.

The mid-span deformation of the timber specimens versus the load is shown in Fig. 9. It was observed that all the specimens presented a brittle failure at mid-span and that the ultimate load resisting capacity is in the range of 8.2–12.1 kN. Such variations are apparent since the timber products are heterogeneous and some natural growth variations and defects exist in the specimens.

The software package ABAQUS was used to develop the finite element (FE) models for the timber boards. Fig. 10 shows a schematic view of the FE model utilized in the study. Taking advantage of symmetry, only a quarter of the specimen was modelled with the material properties of C24 timber material [34] given in Table 3. The FE model consists of a three-dimensional timber specimen as well as one cylindrical support and one cylindrical loading rod, which are modelled as analytical rigid surfaces. The timber specimen has the same dimensions as those used in the experimental tests.

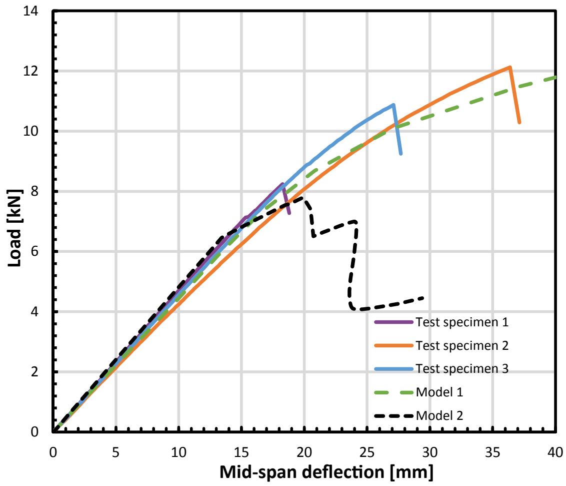

Fig. 13. Comparison between experimental and numerical load–deflection responses.

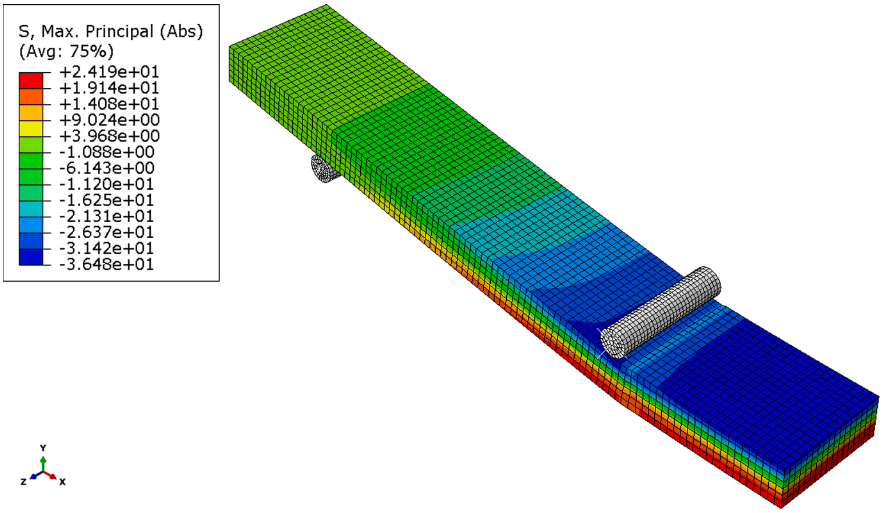

Fig. 14. Stress distribution of timber model at failure load (values in MPa).

Linear hexahedral elements (C3D8R) of ABAQUS with reduced integration were employed to discretize the timber board and the average mesh size was first set to 15 mm. The boundary conditions were modelled using the cylindrical support constrained in all degrees of freedom. The loads were applied as a constant displacement in the vertical direction using the cylindrical rigid body acting on the timber board. The contact between the timber specimen and the cylindrical rigid bodies was defined in both normal and transverse directions with the consideration of Pressure-overclosure “Hard” contact, and the static coefficient of friction equaled to 0.4, respectively. In addition, a relevant symmetric boundary condition was assigned at the symmetric plane.

In Model 1, mesh sensitivity was considered with a convergence study. Since the thickness of the timber element is significantly smaller than its length and width, the thickness was assigned with a minimum number of four elements. Thus, in a first approach, a model with a mesh size of 15 mm was analyzed leading to at least four elements over the thickness of the timber board. Then, the mesh size was subsequently reduced to 2 mm in five different scenarios.

To find a proper mesh size configuration, the results were compared by comparing the deflection accuracy and computing time. Fig. 11 plots the mid-span deflection of the timber board for various mesh sizes. It can be seen that the mesh size affects the analysis to approach the solution that governs the exact response. It can be seen that the coarse mesh gives less accurate deflections at the mid-span of the timber board. However, the fine meshes (2, 3 and 5 mm mesh size) show a very similar pattern for the load–deflection curve and little change in the solution. Thus, 5 mm mesh size is assumed to have converged.

The computing time and the number of finite elements of each mesh scenario are shown in Fig. 12. When the meshing size decreases, the number of element in the model increases. As a result of decreasing meshing size, the solution procedure uses an excessive

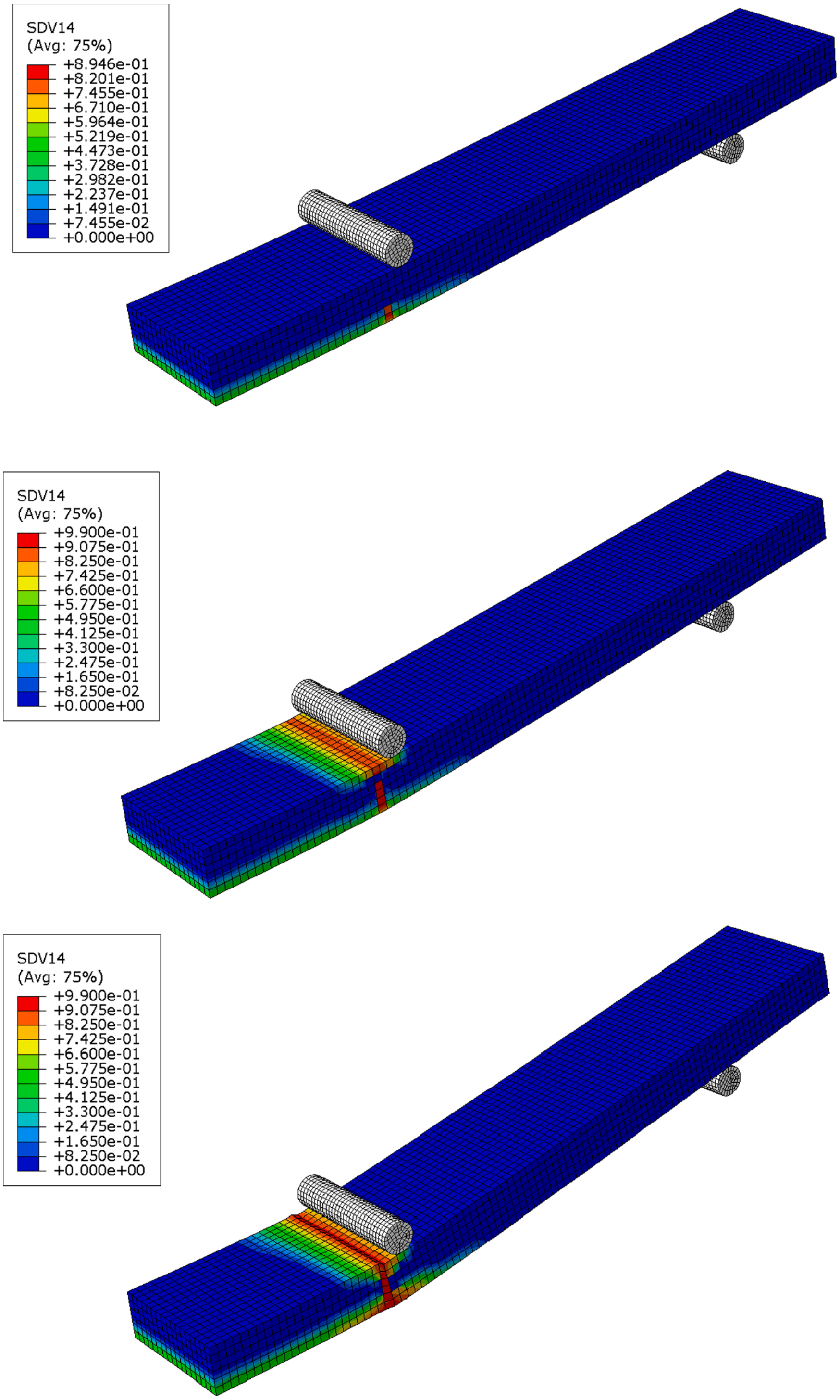

Fig. 15. Damage evolution in the timber model.

number of increments and iteration, and hence the computing time also increases. As a summary of the convergence study, the 5 mm mesh size is almost accurate as of the 2 mm and reduces the computation time by almost 88 percent.

The load–displacement curves obtained from the numerical analysis is illustrated in Fig. 13 and compared with the experimental test results. The stiffness of the FE model is in line with the experimental results in the elastic zone. Overall, a reasonably good correlation between the numerical and experimental results is observable. In Model 1, timber depicts a plateau region due to the plastic yielding, and it grows continuously because of no failure criterion is introduced. It can be seen that the predicted response of Model 2 is

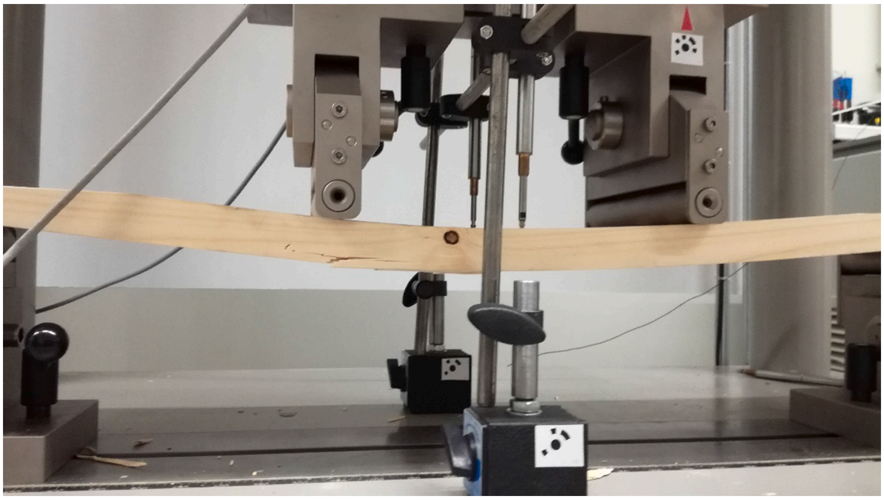

Fig. 16. Failure in timber specimen obtained in bending test experiment.

in good agreement with the experiment because local failure of timber specimen is defined. Therefore, it demonstrates that the proposed material model adequately simulates the non-linear response of the timber element in bending.

Fig. 14 shows the maximum principal stress distribution of the timber specimen in Model 1. It can be seen that the highest stress values are at mid-span which are almost equal to the defined strength of the timber. Therefore, it is clear that the failure in the FE model occurs at mid-span and starts about the same load as in the test results.

Fig. 15 shows the damage evolution in the timber in Model 2. It is clearly seen that first damage occurs in the vicinity of the loading rod. The damaged zone increases with the load increases. Subsequently, the failure occurs at mid-span deflection of 20.2 mm due the fact that damage is highly localized in the vicinity to the loading rod. The predicted failure of the model is in good agreement with the observed rupture in the experiment as shown in Fig. 16. Hence, Model 2 can accurately predict the localized damage in the timber element.

5. Conclusions

Timber is a heterogeneous and orthotropic material. In structural engineering applications, the nonlinear response of timber is typically predicted by phenomenological models and 2D analysis. In this study, a new 3D constitutive model was developed to model nonlinear mechanical response of timber, as elastoplastic orthotropic material. Since there are only a few 3D FE models representing timber behavior available in the literature, the proposed model makes an important addition to the structural timber engineering.

An isotropic hardening elastoplastic model that is combined with Hoffman yield criterion, which defines the anisotropic yield of materials, and combined with anisotropic damage effect in failure criterion was developed and implemented as a user material subroutine UMAT in ABAQUS FE code. The strain hardening of the timber was introduced into the Hoffman criterion using the strength of the material is a function of the equivalent plastic strain. An associated flow rule model based on Hoffman yield criterion and plastic potential was used for the development of the plasticity when the timber under compression. A stress-based continuum damage formulation with four independent failure criteria in tension and compression was used to distinguish the timber response under tension and compression. Three tensile damages in the grain longitudinal, radial and tangential directions was established using the damage factors and fracture energies. ABAQUS provides the development function for users to develop their own material model to complete various material analyses. The FORTRAN syntax was used to program the UMAT which includes the integration procedures using vector formed state variables. The algorithm formulas for calculating the problem were derived from the Newton-Raphson method.

Three timber specimens were tested in bending in order to study their structural behavior. Finite element simulations of timber elements with hardening behavior were carried out and the analysis is validated by comparing with the experimental test results. In addition, the material model developed in this study was validated in the context of uniaxial compressive and tensile loadings by comparing it to the experimental results available in literature. The validation of the developed constitutive model was confirmed.

Declaration of Competing Interest

The authors declare that they have no known competing financial interests or personal relationships that could have appeared to influence the work reported in this paper.

Acknowledgements

This research is in the framework of the project Eco-construction for Sustainable Developments (ECON4SD), supported by the program “*Investissement pour la croissance et l’emploi*”—European Regional Development Fund (2014–2020) (Grant agreement: 2017-02-015-15).

References

[1] J. Porteous, A. Kermani, Timber as a structural material. Structural Timber Design to Eurocode 5, Blackwell, 2007.
[2] A. Padilla-Rivera, B. Amor, P. Blanchet, Evaluating the link between low carbon reductions strategies and its performance in the context of climate change: a carbon footprint of a wood-frame residential building in Quebec, Canada, Sustainability 10 (2715) (2018).
[3] A. Reiterer, S.E. Stanzl-Tschegg, Compressive behaviour of softwood under uniaxial loading at different orientations to the grain, Mech. Mater. 33 (12) (2001) 705–715.
[4] L.F. Sirumbal-Zapata, C. Málaga-Chuquitaype, A.Y. Elghazouli, A three-dimensional plasticity-damage constitutive model for timber under cyclic loads, Comput. Struct. 195 (2018) 47–63.
[5] E. Borgström, Design of timber structures - Structural aspects of timber construction, Swedish Forest Industries Federation, Stockholm, 2016.
[6] A. Harte, Introduction to timber as an engineering material, ICE Manual Constr. Mater. 2 (2009) 707–715.
[7] L. Daudeville, Fracture in spruce: Experiment and numerical analysis by linear and non linear fracture mechanics, Holz als Roh- und Werkstoff 57 (6) (1999) 425–432.
[8] C.J. Chen, T.L. Lee, D.S. Jeng, Finite element modelling for the mechanical behavior of dowel-type timber joints, Comput. Struct. 81 (2003) 2731–2738.
[9] N. Kharouf, G. McClure, I. Smith, Elasto-plastic modelling of wood bolted connections, Comput. Struct. 81 (2003) 747–754.
[10] K. Sawata, M. Yasumura, Estimation of yield and ultimate strengths of bolted timber joints by nonlinear analysis and yield theory, J. Wood Sci. 49 (5) (2003) 383–391.
[11] L. Daudeville, L. Davenne, M. Yasumura, Prediction of the load carrying capacity of bolted timber joints, Wood Sci. Technol. 33 (1) (1999) 15–29.
[12] E. Serrano, Glued-in rods for timber structures — a 3D model and finite element parameter studies, Int. J. Adhes. Adhes. 21 (2) (2001) 115–127.
[13] I. Smith, S. Vasic, Fracture behaviour of softwood, Mech. Mater. 35 (8) (2003) 803–815.
[14] S. Vasic, I. Smith, E. Landis, Finite element techniques and models for wood fracture mechanics, Wood Sci. Technol. 39 (1) (2005) 3–17.
[15] C.L. Santos, A.M.P. De Jesus, J.J.L. Morais, J.L.P.C. Lousada, Quasi-static mechanical behaviour of a double-shear single dowel wood connection, Constr. Build. Mater. 23 (1) (2009) 171–182.
[16] E. Benvenuti, N. Orlando, C. Gebhardt, M. Kaliske, An orthotropic multi-surface damage-plasticity FE-formulation for wood: Part I – Constitutive model, https://www.sciencedirect.com/science/journal/00457949, vol. 240, p. 106350, 2020.
[17] F. Nouri, H.R. Valipour, Moment-rotation model for steel-timber composite connections with slab continuity steel rods, J. Constr. Steel Res. 173 (2020), 106257.
[18] A.M.P.G. Dias, J.W. Van de Kuilen, S. Lopes, H. Cruz, A non-linear 3D FEM model to simulate timber-concrete joints, Adv. Eng. Softw. 38 (8-9) (2007) 522–530.
[19] D.M. Moses, H.G.L. Prion, Stress and failure analysis of wood composites: a new model, Compos. B Eng. 35 (3) (2004) 251–261.
[20] M. Patton-Mallory, S.M. Cramer, F.W. Smith, P.J. Pellicane, Nonlinear material model for analysis of bolted wood connections, J. Struct. Eng. 123 (8) (1997) 1063–1070.
[21] R. Hill, A theory of the yielding and plastic flow of anisotropic metals, Proc. R. Soc. Lond. Ser. A 193 (1948) 281–297.
[22] S.W. Tsai, E.M. Wu, A general theory of strength for anistropic materials, J. Compos. Mater. 5 (1) (1971) 58–80.
[23] O. Hoffman, The brittle strength of orthotropic materials, J. Compos. 1 (2) (1967) 200–206.
[24] M. Oudjene, M. Khalifa, Elasto-plastic constitutive law for wood behavior under compressive loadings, Constr. Build. Mater. 23 (2009) 3359–3366.
[25] A. Bouchair, A. Vergne, An application of the Tsai criterion as a plastic law for timber bolted joint modelling, Wood Sci. Technol. 30 (1995) 3–19.
[26] P.L. Clouston, F. Lam, Computational modeling of strand-based wood composites, J. Eng. Mech. 127 (8) (2001) 844–851.
[27] B.H. Xu, M. Taazount, A. Bouchaïr, P. Racher, Numerical 3D finite element modelling and experimental tests for dowel-type timber joints, Constr. Build. Mater. 23 (2009) 3043–3052.
[28] M. Gharib, A. Hassanieh, H. Valipour, M.A. Bradford, Three-dimensional constitutive modelling of arbitrarily orientated timber based on continuum damage mechanics, Finite Elem. Anal. Des. 135 (2017) 79–90.
[29] M. Lukacevic, W. Lederer, J. Füssl, A microstructure-based multisurface failure criterion for the description of brittle and ductile failure mechanisms of clear-wood, Eng. Facture Mech. 176 (2017) 83–99.
[30] P. Mackenzie-Helnwein, H.W. Müllner, J. Eberhardsteiner, H.A. Mang, Analysis of layered wooden shells using an orthotropic elasto-plastic model for multi-axial loading of clear spruce wood, Comput. Methods Appl. Mech. Eng. 194 (21–24) (2005) 2661–2685.
[31] P. Mackenzie-Helnwein, J. Eberhardsteiner, H.A. Mang, A multi-surface plasticity model for clear wood and its application to the finite element analysis of structural details, Comput. Mech. 31 (1-2) (2003) 204–218.
[32] J. Schmidt, M. Kaliske, Models for numerical failure analysis of wooden structures, Eng. Struct. 31 (2) (2009) 571–579.
[33] C. Sandhaas, J.-W. Van de Kuilen, H.J. Blass, Constitutive model for wood based on continuum damage mechanics, in: 12th World Conference on Timber Engineering, Auckland, 2012.
[34] C. Sandhaas, J. Van de Kuilen, Material model for wood, Heron 58 (2013) 173–194.
[35] N. Orlando, Y. Taddia, E. Benvenuti, B. Pizzo, C. Alessandri, End-repair of timber beams with laterally-loaded glued-in rods: experimental trials and failure prediction through modelling, Constr. Build. Mater. 195 (2019) 623–637.
[36] B.-H. Xu, A. Bouchaïr, P. Racher, Appropriate wood constitutive law for simulation of nonlinear behavior of timber joints, J. Mater. Civ. Eng. 26 (6) (2014) 04014004.
[37] A. Khennane, M. Khelifa, L. Bleron, J. Viguier, Numerical modelling of ductile damage evolution in tensile and bending tests of timber structures, Mech. Mater. 68 (2014) 228–236.
[38] M. Khelifa, A. Khennane, M. El Ganaoui, A. Celzard, Numerical damage prediction in dowel connections of wooden structures, Mater. Strucut. 49 (2016) 1829–1840.
[39] T.-T. Tran, V.-D. Thi, M. Khelifa, M. Oudjene, Y. Rogaume, A constitutive numerical modelling of hybrid-based timber beams with partial composite action, Constr. Build. Mater. 178 (2018) 462–472.
[40] E. Benvenuti, N. Orlando, C. Gebhardt, M. Kaliske, An orthotropic multi-surface damage-plasticity FE-formulation for wood: Part II – Numerical applications, Comput. Struct. 240 (2020), 106351.
[41] N.T. Mascia, F.A.R. Lahr, Remarks on orthotropic elastic models applied to wood, Mater. Res. 9 (3) (2006) 301–310.
[42] N.T. Mascia, L. Vanalli, Evaluation of the coefficients of mutual influence of wood through off-axis compression tests, Constr. Build. Mater. 30 (2012) 522–528.
[43] N. Khorsandnia, H.R. Valipour, K. Crews, Nonlinear finite element analysis of timber beams and joints using the layered approach and hypoelastic constitutive law, Eng. Strucut. 46 (2013) 606–614.

[44] ABAQUS, Theory manual, version 6.14, Dassault Systèmes Simulia Corp., 2018.
[45] J.C.J. Schellekens, R. De Borst, The use of the Hoffman yield criterion in finite element analysis of anistropic composites, Comput. Struct. 37 (6) (1990) 1087–1096.
[46] J.-Y. Lee, J.-W. Lee, M.-G. Lee, F. Barlat, An application of homogeneous anisotropic hardening to springback prediction in pre-strained U-draw/bending, Int. J. Solids Struct. 49 (25) (2012) 3562–3572.
[47] J.C. Simo, J.W. Ju, Strain- and stress-based continuum damage models-I. Formulation, Int. J. Solids Struct. 23 (7) (1987) 821–840.
[48] A.i. Shigang, F. Daining, H.e. Rujie, P. Yongmao, Effect of manufacturing defects on mechanical properties and failure features of 3D orthogonal woven C/C composites, Compos. B Eng. 71 (2015) 113–121.
[49] M. Wang, X. Song, X. Gu, Three-Dimensional combined elastic-plastic and damage model for nonlinear analysis of wood, J. Struct. Eng. 144 (8) (2018) 04018103.
[50] J.L. Chaboche, F. Feyel, Y. Monerie, Interface debonding models: a viscous regularization with a limited rate dependency, Int. J. Solids Struct. 38 (18) (2001) 3127–3160.
[51] I. Lapczyk, J.A. Hurtado, Progressive damage modeling in fiber-reinforced materials, Compos. A Appl. Sci. Manuf. 38 (11) (2007) 2333–2341.
[52] D.R.J. Owen, E. Hinton, Finite Elements in Plasticity, Theory and Practice, Pineridge Press, Swansea, 1980.
[53] V. Karagiannis, C. Malaga-Chuquitaype, A.Y. Elghazouli, Modified foundation modelling of dowel embedment in glulam connections, Constr. Build. Mater. 102 (2016) 1168–1179.
[54] S. Maiti, L. Gibson, M. Ashby, Deformation and energy absorption diagrams for cellular solids, Acta Metall. 32 (11) (1984) 1963–1975.